Self-Association of the Anionic Form of the DNA-Binding Anticancer Drug Mithramycin

ARTICLE *in* THE JOURNAL OF PHYSICAL CHEMISTRY B · APRIL 2008

Impact Factor: 3.3 · DOI: 10.1021/jp710503g · Source: PubMed

Self-Association of the Anionic Form of the DNA-Binding Anticancer Drug Mithramycin

Shibojyoti Lahiri, Pukhrambam Grihanjali Devi, Parijat Majumder, Suman Das,† and Dipak Dasgupta*

Biophysics Division, Saha Institute of Nuclear Physics, 1/AF Sector-1, Bidhannagar, Kolkata-700064, India

Received: October 31, 2007; In Final Form: December 22, 2007

The aqueous-phase self-association of mithramycin (MTR), an aureolic acid anticancer antibiotic, has been studied using different spectroscopic techniques such as absorption, fluorescence, circular dichroism, and ^{1}H nuclear magnetic resonance spectroscopy. Results from these studies indicate self-association of the anionic antibiotic at pH 8.0 over a concentration range from micromolar to millimolar. These results could be ascribed to the following steps of self-association: $M + M \leftrightarrows M_2$, $M_2 + M \leftrightarrows M_3$, and $M_3 + M \leftrightarrows M_4$, where M, M_2, M_3, and M_4 represent the monomer, dimer, trimer, and tetramer of mithramycin, respectively. Dynamic light scattering and isothermal titration calorimetry studies also support aggregation. In contrast, an insignificant extent of self-association is found for the neutral drug (at pH 3.5) and the $[(MTR)_2Mg^{2+}]$ complex (at pH 8.0). Analysis of 2D NMR spectra of 1 mM MTR suggests that the sugar moieties play a role in the self-association process. Self-association of the drug might occur either via hydrophobic interaction of the sugar residues among themselves or water-mediated hydrogen bond formation between sugar residue(s). On the other hand, absence of a significant upfield shift of the aromatic protons from 100 μM to 1 mM MTR suggests against the possibility of stacking interactions between the aromatic rings as a stabilizing force for the formation of the dimer and higher oligomers.

1. Introduction

Mithramycin (MTR) (Figure 1) is a naturally occurring antibiotic synthesized by *Streptomyces plicatus*[1] and *Streptomyces argillaceus*. It consists of a tricyclic aromatic moiety, the aglycone, with two aliphatic side chains at C3 and C7. Either side of the aglycone ring is connected to six-membered sugar residues via *O*-glycosidic linkages.[2] Different studies have established that this antibiotic inhibits both in vivo and in vitro transcription via reversible interaction with DNA,[1−5] in the presence of bivalent metal ions like Mg^{2+}.

MTR finds its use in the treatment of various neoplastic diseases like chronic mylogenous leukemia, testicular carcinoma, and Paget's disease of bones.[1] It also inhibits the expression of proto-oncogenes like *c-myc*.[6] In recent years, there has been an upsurge of interest in exploring the therapeutic potential of generic drugs like MTR in diseases besides cancer. Reports have shown that MTR induces fetal hemoglobin production in normal and thalassemic human erythroid precursor cells.[7] It down regulates proinflammatory cytokine-induced matrix metalloproteinase gene expression in articular chondrocytes.[8] MTR also prolongs survival in a mouse model of Huntington's disease (R6/2), its potency being 29.1% greater than any single agent reported to date.[9] A recent report has shown that MTR inhibits DNA methyltransferase and the metastasis potential of lung cancer cells.[10] These studies propose that promoter binding followed by alteration of gene expression is the predominant pathway of action of the drug, and the same is utilized for a therapeutic cause. The recent spate of reports emphasizes the importance of understanding the chemical biology of the function of the drug.

In our laboratory, we aim to understand the molecular basis of the biological function of the drug. A necessary requirement to achieve this objective is the characterization of the antibiotic in the absence of any metal ion and biopolymer. Here, we report our studies on the self-association of the antibiotic over a concentration ranging from micromolar to millimolar at pH 8.0, where MTR is in the anionic form. Self-association of MTR would play an important role in its storage, biological action, and gene expression of its biosynthetic gene cluster in *Streptomyces* species. Self-association property of MTR might lead to altered storage efficiency in the microorganism, which, in turn, can alter the gene expression profile through feedback loops.

We have employed spectroscopic techniques such as absorbance, fluorescence, circular dichroism (CD), dynamic light scattering (DLS), and nuclear magnetic resonance (NMR) to elucidate and characterize the self-association property of MTR. Apart from these techniques, isothermal titration calorimetry (ITC) was used to identify the self-association process, whereby the variable heat of dilution of the drug is indicative of the presence of species in different states of aggregation.

The drug molecule at and above physiological pH is anionic. Therefore, in order to elucidate the role of electrostatic charges in self-association, a control calorimetric titration was performed with the neutral drug at pH 3.5 because the p*K*a of MTR is 5.0. Since the active molecular species that interacts with DNA is the drug−metal complex $[(MTR)_2Mg^{2+}]$,[11] we compared the results with a drug dimer complex with Mg^{2+}.

The results show that the anionic drug associates extensively above physiological pH, while the drug−metal complex and the neutral drug molecule do not associate to any significant extent.

2. Experimental Methods

2.1. Materials. MTR was obtained from Sigma Chemical Co., U.S.A., and also from MP Biomedicals, France. Hydro-

* To whom correspondence should be addressed. E-mail: dipak.dasgupta@saha.ac.in. Tel.: +91-033-23370379. Fax: +91-033-23374637.
† Present address: Department of Chemistry, Maulana Azad College, 8 Rafi Ahmed Kidwai Road, Kolkata 700013, India.

10.1021/jp710503g CCC: $40.75
Published on Web 02/19/2008

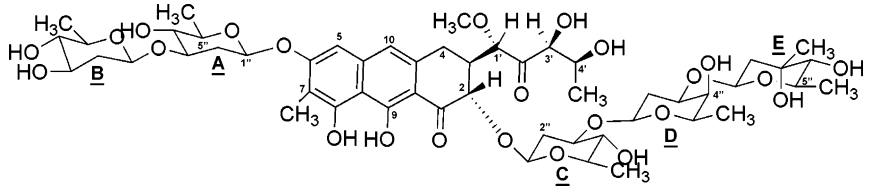

Figure 1. Chemical structure of MTR.

chloric acid (HCl), ethidium bromide (EtBr), and magnesium chloride ($MgCl_2$) were also obtained from Sigma Chemical Co., U.S.A. Tris was purchased from Merck, India, and sodium acetate (CH_3COONa) was purchased from Merck, Germany. Disodium hydrogen phosphate was obtained from Merck, India, and sodium dihydrogen phosphate was from Sisco Research Laboratories (SRL) Pvt. Ltd., India. All reagents used were of spectroscopy grade, and the solutions were prepared in Milli-Q (Synergy, Millipore, U.S.A.) water after filtration through a 0.22 μm filter. Disposable plastic cuvettes from Volex Plasticwares, Italy, were used for DLS measurements.

2.2. Buffers. All experiments were performed in 50 mM Tris−HCl (pH 8.0), unless otherwise stated. The ITC experiment involving the neutral form of the drug molecule was performed in 50 mM sodium acetate−acetic acid buffer (pH 3.5). For the NMR experiments, 20 mM phosphate buffer (NaH_2PO_4−Na_2HPO_4) at pH 8.0 was used.

2.3. Preparation of MTR. A solution of MTR was prepared in 50 mM Tris−HCl (pH 8.0), and the concentration was checked from absorbance measurements at 400 nm. An extinction coefficient of 10^4 M^{-1} cm^{-1} at 400 nm was used for the concentration range of 10−20 μM.

2.4. Visible Spectroscopy. All visible absorbance spectra were recorded in a Cecil 7500 UV−visible spectrophotometer (with built-in DataStream CE 7000 Series software). Absorbance spectra of different concentrations of MTR and its Mg^{2+} complex (complex II) in 50 mM Tris−HCl (pH 8.0) were measured at 25 °C in quartz cuvettes of 1 cm path length, and the extinction coefficient of 10^4 M^{-1} cm^{-1} at 400 nm was taken over the concentration range. The spectra shown in the results contain a normalized absorbance (A/A_{max}) as a function of wavelength, where A is the absorbance and A_{max} is the absorbance at the peak.

2.5. Fluorescence Spectroscopy. Fluorescence spectra of MTR at different concentrations were recorded in a Perkin-Elmer LS 55 luminescence spectrometer using a quartz cell of 1 cm path length (λ_{ex} = 470 nm). The fluorescence intensity values at 540 nm were noted in each case. Fluorescence measurements were done in the concentration range of 2−30 μM to ascertain self-association. The upper limit of the concentration was limited to an absorbance of 0.02.[12] Both the excitation and the emission slit widths were kept at 10 nm.

2.6. Isothermal Titration Calorimetry (ITC). The heat of dilution of different species of the drug molecule was measured in a VP−ITC microcalorimeter (MicroCal Inc., U.S.A.) using the built-in VP Viewer 2000 software with Origin 7.0. In all experiments, MTR was taken in the syringe (280 μM) and injected into the cell containing 50 mM Tris−HCl (pH 8.0). All experiments were performed at 25 °C with the syringe having a stirring speed of 307 rpm. All solutions were filtered and degassed extensively before each experiment. Corrected enthalpies were calculated after subtracting the enthalpy change due to mixing of the buffer−buffer in each case.

2.7. Dynamic Light Scattering (DLS). DLS measurements were performed using a ZetaSizer Nano Series (Nano S) machine from Malvern Instruments, U.K., using disposable cuvettes of 1 cm path length. The samples were filtered through Millipore Millex GV filters (Pore Size = 0.22 micron) and incubated at 25 °C for at least 30 min before the start of the experiments. A further equilibration time of 5 min was allowed for the samples after loading onto the DLS machine. The DLS data were analyzed by Dispersion Technology Software (DTS). The size of the species present in the solution is expressed in terms of its average hydrodynamic diameter, calculated from three measurements in each case.

2.8. Circular Dichroism (CD) Spectroscopy. We have employed CD spectroscopy to quantitatively evaluate the aggregation of molecular species of MTR over broad concentration ranges. Circular dichroism spectra were recorded in a Jasco J720 spectropolarimeter using a quartz cuvette of 1 cm path length. Data were analyzed using the Jasco CD Standard Analysis software. The change of ellipticity as a function of concentration has been plotted at different wavelengths (275, 393, and 412 nm for the anionic drug and 321 and 443 nm for the drug−metal complex). These wavelengths were chosen as the changes in CD at these wavelengths were most pronounced for the two systems.

2.9. ^{1}H NMR Spectroscopy. NMR spectra were recorded at 25 °C in a Bruker 600 UltraShield NMR machine; 10% D_2O was used for external locking. 1D NMR spectra for MTR (100 μM, 300 μM, and 1 mM) were recorded. For the [$(MTR)_2Mg^{2+}$] complex, each concentration of MTR was preincubated with 10 mM Mg^{2+} for at least 30 min before the spectra was recorded. 2D ^{1}H NMR (TOCSY and NOESY) spectra were recorded for MTR (1 mM) and the [$(MTR)_2Mg^{2+}$] complex (1 mM MTR containing 10 mM Mg^{2+}). The 2D spectra were recorded for ∼16 h. A mixing time of 400 ms was used in each case. All samples were prepared in 20 mM phosphate buffer (pH 8.0). Data were analyzed using Bruker TopSpin 1.3 software.

3. Results

3.1. Absorbance Measurements of Anionic MTR and the [$(MTR)_2Mg^{2+}$] Complex. Figure 2A and B shows the representative normalized absorption spectra of anionic MTR and the [$(MTR)_2Mg^{2+}$] complex at three different concentrations. Non-overlap of the three spectra of the anionic drug at different concentrations suggests aggregation with an increase in concentration. A red shift of the peak with increasing concentration is the notable feature. On the contrary, in case of the drug−metal complex, the spectra are overlapping throughout the concentration range (Figure 2B) investigated and are indicative of insignificant association.

3.2. Fluorescence Titration. Comparison of the normalized fluorescence spectra (Figure 3A) suggests an alteration in the state of association with an increase in concentration for the anionic drug. Normalized spectra show quenching upon an increase in concentration to 30 μM. This is further corroborated by a deviation from linearity of the intensity values with respect

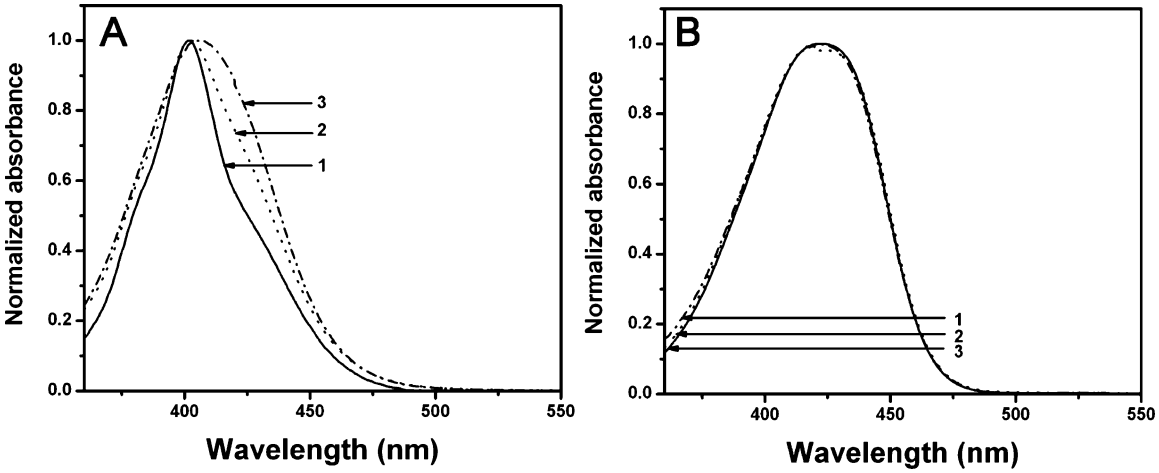

Figure 2. Absorption spectra of (A) anionic MTR and (B) the [$(MTR)_2Mg^{2+}$] complex in 50 mM Tris−HCl buffer, pH 8.0, at 25 °C at concentrations of 5 μM, curve 1; 60 μM, curve 2; and 200 μM, curve 3.

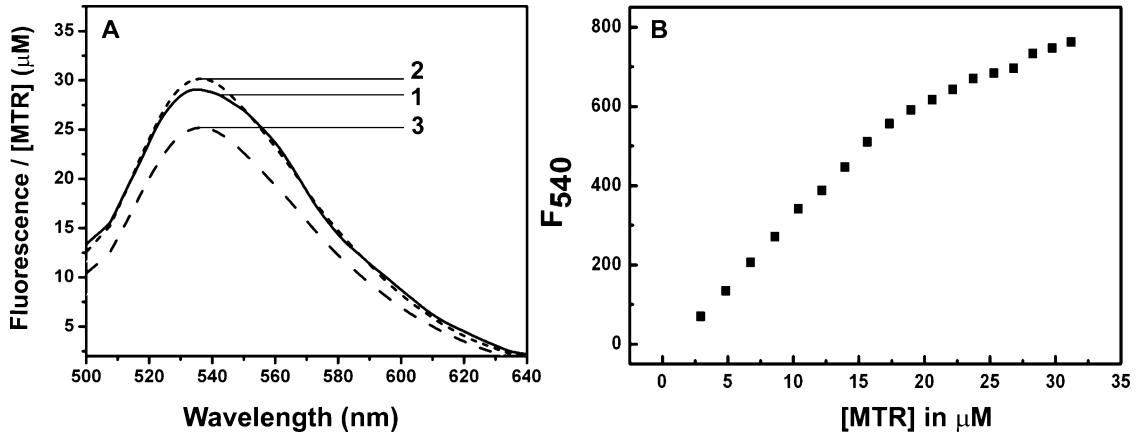

Figure 3. (A) Plot of fluorescence spectra (normalized per micromolar MTR) in 50 mM Tris−HCl buffer, pH 8.0, at 25 °C. Three representative concentrations (4.9 μM, curve 1; 20.6 μM, curve 2; and 29.8 μM, curve 3) are shown. (B) Plot of the fluorescence intensity at 540 nm (λ_{ex} = 470 nm) as a function of the concentration of MTR; the excitation and emission slit widths are 10 nm.

to concentration (Figure 3B). On the other hand, the change in the fluorescence spectra as a function of concentration is not significant in case of the [$(MTR)_2Mg^{2+}$] complex (data not shown).

3.3. ITC Measurements of the Heat of Dilution. The phenomenon of self-association of MTR at lower concentration ranges was examined thermodynamically by monitoring the heat of dilution as a function of concentration. For a molecular species that remains the same during the course of its dilution, the molar heat of dilution should remain invariant with concentration. However, in contrast, anionic MTR exhibits a concentration-dependent change in the molar heat of dilution (Figure 4). EtBr serves as the control (Figure 4), where insignificant alteration in the heat of dilution implies the presence of a single species throughout the course of dilution. Scrutiny of the two curves shows that there is a change in the state of aggregation within the concentration range of 0−30 μM for the anionic drug. The non-overlap of the normalized absorbance and fluorescence spectra at different concentrations supports the observation. The neutral drug at pH 3.5 does not show significant variation in the molar heat of dilution (Figure 4). However, the ITC profile of MTR shows a varying heat of dilution with concentration arising from self-association. We did not try the ITC approach for the [$(MTR)_2Mg^{2+}$] complex because the enthalpy of hydration of the hydrated Mg^{2+} ion could lead to a potential artifact.

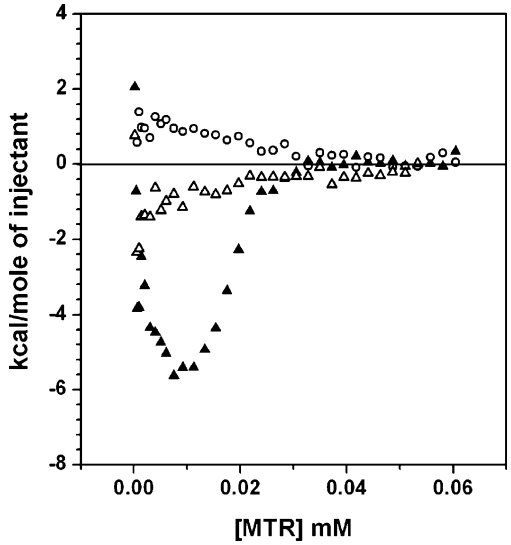

Figure 4. Calorimetric titration of anionic MTR (▲) and EtBr (△) in 50 mM Tris−HCl, pH 8.0, at 25 °C and of neutral MTR in a sodium acetate−acetic acid buffer (pH 3.5) (○) at 25 °C.

3.4. Dynamic Light Scattering. In order to quantitate and get first-hand information about the state(s) of association in the concentration ranges mentioned above, we examined our system by means of dynamic light scattering (DLS). Figure 5A

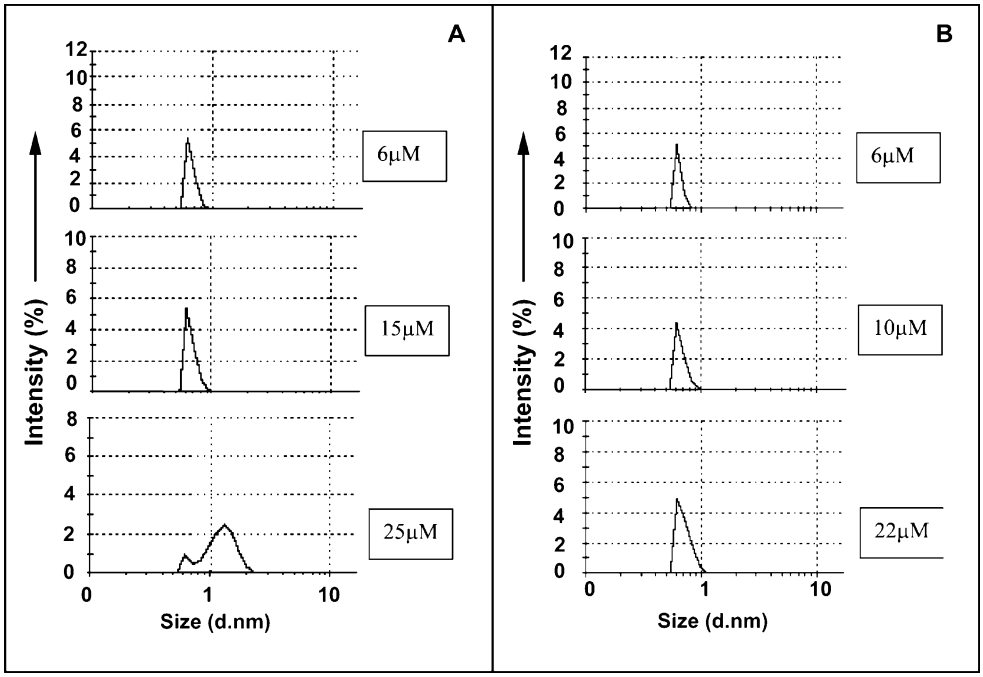

Figure 5. Size distribution by intensity of the molecular species as measured by dynamic light scattering (DLS). (A) DLS measurements of anionic MTR molecule at three representative concentrations. (B) DLS measurements of the $[(MTR)_2Mg^{2+}]$ complex at three representative concentrations of MTR containing 10 mM Mg^{2+} in 50 mM Tris−HCl, pH 8.0, at 25 °C.

represents the size distribution of MTR in the concentration range of 6−25 μM as a function of its scattering intensity. The average hydrodynamic diameter of the molecular species present in the concentration range of 6−15 μM for the anionic MTR is 0.66 nm. Above this concentration, at 25 μM, there is a distinct change in the number of molecular species present in the system. The intensity of the molecular species having a diameter of 0.66 nm decreases while there is an emergence of a new molecular species with a higher average diameter of 1.28 nm. The results indicate the formation of a higher-ordered aggregate having a distinct physical existence (Table 1). DLS measurements of the $[(MTR)_2Mg^{2+}]$ complex do not show any alteration in the state of association (Figure 5B, Table 1) over the concentration range of 0−25 μM.

3.5. CD Spectroscopic Measurements at Higher Concentrations of MTR. Figure 6A shows concentration-dependent CD spectra of anionic MTR in the visible range. There is a change in the shape of the spectra and crossover wavelength upon an increase in the concentration from 16 to 103 μM. Further increase does not alter the spectral shape significantly. The splitting of bands with two peaks becomes apparent at higher concentration. Plots of the ellipticity as a function of concentration at different wavelengths (275 nm, Figure 6B; 412 nm, Figure 6C; and 393 nm, Figure 6D) for the anionic drug show two breaks in each case. The nature of the plot indicates three types of species over the total concentration range. Therefore, in order to describe the observed association throughout the entire concentration range and on the basis of the assumption of a dimerization process, we propose a tetrameric model of self-association of MTR

$M + M \leftrightarrows M_2$	association constant = K_1
$M_2 + M \leftrightarrows M_3$	association constant = K_2
$M_3 + M \leftrightarrows M_4$	association constant = K_3
$4M \leftrightarrows M_4$	association constant = K

TABLE 1: Mean Hydrodynamic Diameter of the Existing Drug Species in 50 mM Tris−HCl, pH 8.0, at 25 °C as a Function of Its Concentration as Measured by DLS

system	MTR			$[(MTR)_2Mg^{2+}]$		
concentration (μM)	6	15	25	6	10	22
mean diameter (nm)	0.658	0.669	0.655/1.280	0.639	0.668	0.707

with three association constants, denoted as K_1, K_2, and K_3 (where $K = K_1 \times K_2 \times K_3$). M, M_2, M_3, and M_4 represent the monomer, dimer, trimer, and tetramer of mithramycin, respectively. For the initial dimerization process, we have

$$K_1 = \frac{[M_2]}{[M]^2} \tag{1}$$

which, when expressed in terms of the total concentration of MTR (C_0), becomes

$$K_1 = \frac{(C_0 - [M])}{2[M]^2} \tag{2}$$

Solving the above equation for the monomer concentration, we have

$$[M] = (4K)^{-1}(-1 + \sqrt{1 + 8KC_0}) \tag{3}$$

As reported earlier,[13] the following relation connects the molar ellipticity of the monomer and dimer

$$\Delta\epsilon = C_0^{-1}[[M]\Delta\epsilon_M + 0.5\{C_0 - [M]\}\Delta\epsilon_D] \tag{4}$$

for the dimerization process. Here, $\Delta\epsilon$ = the apparent molar CD absorption coefficient, which can be defined as the measured CD divided by the total MTR concentration; $\Delta\epsilon_M$ and $\Delta\epsilon_D$ are the same for the monomer and dimer, respectively. Using the above relation, we calculated the values of $\Delta\epsilon$, $\Delta\epsilon_M$, and $\Delta\epsilon_D$ from the measured CD values at different concentrations. Apparent molar CD absorption coefficients for the trimerization

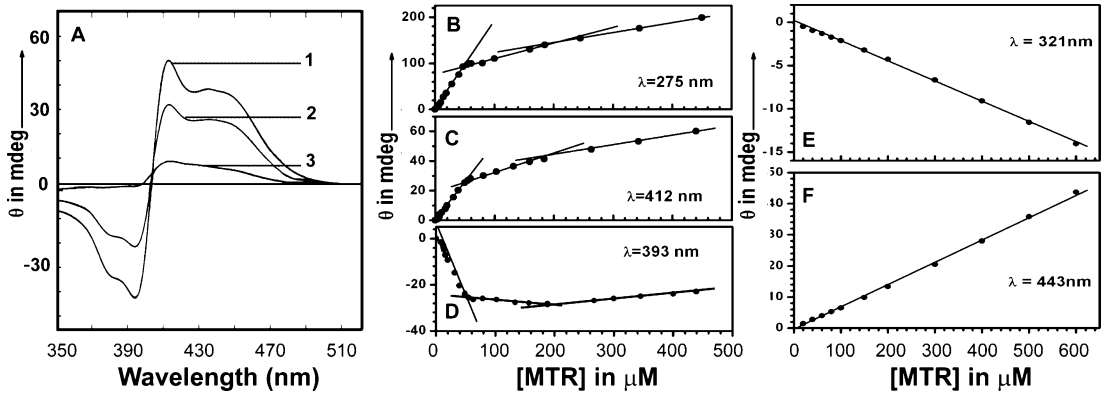

Figure 6. (A) CD spectra of MTR at different concentrations of the drug (342 μM, curve 1; 103 μM, curve 2; and 16 μM, curve 3) in 50 mM Tris−HCl, pH 8.0, at 25 °C. Plot of the observed ellipticity of MTR at (B) 275 nm, (C) 412 nm, and (D) 393 nm and that of the $[(MTR)_2Mg^{2+}]$ complex at (E) 321 nm and (F) 443 nm, as a function of its concentration.

TABLE 2: Values of the Association Constant of Different Orders of Association of MTR in 50 mM Tris−HCl, pH 8.0, at 25 °C

reaction	association constants
$M + M \leftrightarrows M_2$	$K_1 = 1.893\ \mu M^{-1}$
$M_2 + M \leftrightarrows M_3$	$K_2 = 0.013\ nM^{-1}$
$M_3 + M \leftrightarrows M_4$	$K_3 = 0.563\ nM^{-1}$

and tetramerization were calculated taking data from higher concentrations in the CD experiments.

A combination of eqs 4 and 3 enabled us to calculate the association constant for the dimerization process (Table 2). Association constants for other higher-order associations (K_2, K_3) were calculated from expressions of K_2 and K_3, taking data from concentrations higher than 50 μM and considering contributions from the entire concentration range. From the values of the association constants, we see that the predominant process at the lower concentration range is a dimerization process, as is also evident from other experimental observations described previously. The higher-order associations can be attributed to associations effected by the initially formed dimeric species.

In contrast, no appreciable change in the type of molecular species can be observed in case of the drug−metal complex (Figure 6E and F).

3.6. NMR Spectroscopic Measurements. *Anionic MTR Molecule:* Chemical shift values of the drug are found to be in good agreement with previously reported NMR data for the structural elucidation of MTR.[14,15] 1D and 2D NMR spectra were used to assign proton resonances (Table 3) and identify conformational changes, if any, of the drug during the self-association process. Figure 7A shows a full-scale representation of 1D NMR data of anionic MTR at three different concentrations. Detailed investigation of the spectra reveals significant changes of δ values for some of the protons in a concentration-dependent manner (Figure 7B and C).

In order to show the regions of the molecule experiencing a differential environment as a result of self-association, we have selected five marker protons from each portion of the molecule: C3−H and C7−CH_3 (from the aromatic aglycone part), C4′−CH_3 (from the acyclic part of MTR), and EC5″−CH_3 and CC1″−H (from the trisaccharide moiety). The chemical shifts of these protons with increasing concentrations of the anionic drug and $[(MTR)_2Mg^{2+}]$ complex are given in Table 4. An examination of the table shows that the chemical shift changes, if any, of the above marker protons are pronounced in the case of the anionic drug molecule. This trend is consistent with our data from other techniques.

TABLE 3: Chemical Shift Values of Some Protons of MTR (1 mM) and $[(MTR)_2Mg^{2+}]$ (1 mM MTR in the Presence of 10 mM Mg^{2+}) in 20 mM Phosphate Buffer, pH 8.0. at 25 °C

	δ values (ppm)	
protons	anionic MTR	$[(MTR)_2Mg^{2+}]$
C2−H	5.25	5.4
C3−H	1.504	1.5
C4−H(s)	2.15 and 2.46	2.4 and 2.6
C5−H	5.836	5.2
C7−CH_3	1.946	2.048
C10−H	6.3	6.45
C1′−H	3.34	3.3
C1′−OCH_3	3.29	3.265
C3′−H	4.2	4.2
acyclic OH (C3′ and C4′)	6.45 and 6.62	6.6
C4′−H	4.1	4.1
C4′− CH_3	1.17	1.166
sugar C1″−H(a−e)	5.2−5.4	5.0−5.2
sugar C5″−CH_3	1.341/1.351	1.356
sugar H(s)	0.88−2.0	0.7−2.0

The δ value of C7−CH_3 protons shows a distinct upfield shift from 2.096 to 1.946 ppm (Figure 7B) with increasing concentration of the anionic drug molecule from 100 μM to 1 mM. It implies an increase in the shielding effect of the CH_3 protons. As the methyl protons lie outside of the aromatic ring current, the upfield shift can be attributed to an increase in the shielding effect due to the proximity of sugar residues with respect to another anionic drug molecule. This observation is further confirmed from the 2D NMR data (NOESY), where NOESY connectivity shows up between C7−CH_3 and a sugar proton (2.0, 0.09), (DC6″−H, ref 15) (see Supporting Information, Figure S1A). It supports the involvement of sugar residues with the other molecules. On the contrary, we see no appreciable change in the δ values of C3−H and the other aromatic protons, C5−H and C10−H, which rules out the possibility of a stacking interaction in the process of self-association. We could arrive at the same conclusion through ITC measurements of both the anionic drug as well as the neutral drug.

The acyclic part of the molecule is represented by C4′−CH_3 protons (see Supporting Information, Figure S2A), which show an upfield shift as we go from 100 to 300 μM but remains constant thereafter. The C4′−OH and C3′−OH of MTR show NOESY contacts (see Supporting Information, Figure S1B) with the sugar C1″−H(e) and C1″−H(a) of another MTR molecule (6.6, 5.4 and 6.4, 5.2, respectively), which indicate the involvement of the sugar moieties in the process of concentration-dependent association of MTR. The E sugar proton shows significant upfield shifts (Figure 7C). The C1″−H of the C sugar

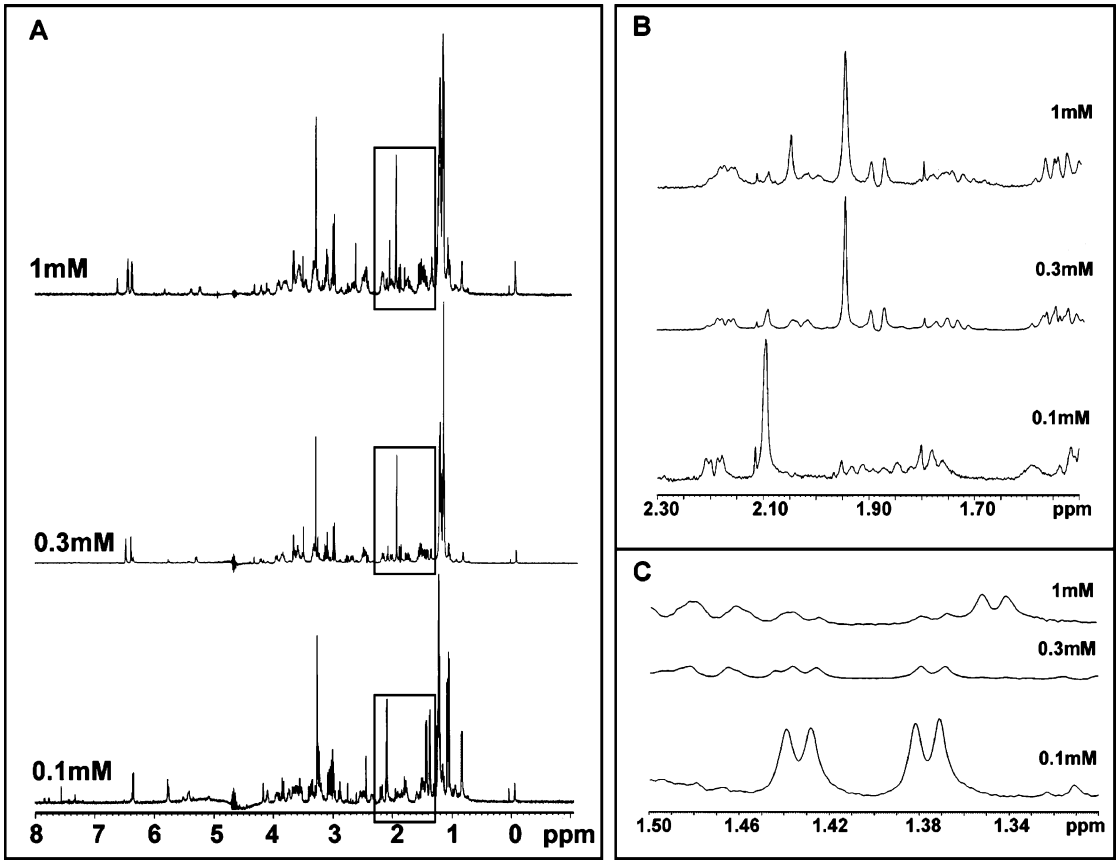

Figure 7. (A) 1D ^{1}H NMR spectra of anionic MTR at 1, 0.3, and 0.1 mM (0−8 ppm) in 20 mM phosphate buffer, pH 8.0, at 25 °C. (B) Expanded region (1.5−2.3 ppm) to show the concentration dependence of the δ value of C7−CH_3. (C) Expanded region (1.3−1.5 ppm) to show the concentration dependence of the δ value of EC5″−CH_3.

TABLE 4: Chemical Shift Values of the Marker Protons for the Anionic Drug and the Drug−Metal Complex in 20 mM Phosphate Buffer, pH 8.0, at 25 °C

		chemical shift values δ (ppm)				
system	conc (mM)	C7−CH_3	C3−H	C4′−CH_3	EC5″−CH_3	CC1″−H
anionic MTR	0.1	2.096	1.5	1.218	1.371/1.382	5.414/5.433
	0.3	1.948	1.5	1.17	1.372/1.385	5.289/5.304
	1.0	1.946	1.5	1.17	1.341/1.351	5.23/5.253
[$(MTR)_2Mg^{2+}$]	0.1	2.057	1.49	1.177	1.359/1.369	5.201/5.186
	0.3	2.051	1.49	1.172	1.357/1.367	5.184/5.170
	1.0	2.048	1.5	1.166	1.356/1.366	5.15

does not show an appreciable shift (see Supporting Information, Figure S2B) upon moving from 100 to 300 μM but experiences an upfield shift thereafter, further confirming our hypothesis.

[$(MTR)_2Mg^{2+}$] Complex: Figure 8A represents the 1D NMR spectra for the [$(MTR)_2Mg^{2+}$] complex. In case of the complex, the δ value of the C7−CH_3 proton does not show any appreciable shift (Figure 8B, Table 4), indicating the absence of a shielding effect due to other approaching molecules toward that particular region of the molecule. The same is applicable for the acyclic part (C4′−CH_3) (see Supporting Information, Figure S2C) as well as the EC5″−CH_3 protons (Figure 8C). However, a significant observation is the distinct upfield shift of the δ values of the CC1″−H (5.2−5.15) (see Supporting Information, Figure S2D). This particular proton lies in the vicinity of the Mg^{2+} ion coordination sphere in the [$(MTR)_2Mg^{2+}$] complex, as can be viewed from the 3D structure of the drug−metal complex (NCBI structure, ID: 146D). This makes the sugar proton more shielded than its counterpart in the anionic drug molecule as it experiences an electrostatic repulsion from the Mg^{2+} ion in the complex. Another important observation is the appearance of many NOE cross-peaks (see Supporting Information, Figure S3) between the sugar protons within the complex, but no such NOESY contacts could be assigned to any coupling of the protons of one complex to that of the other complex. It is evident from the above results that the drug−metal complex does not associate to the same extent as that of the anionic drug. This finding correlates well with our earlier observations.

4. Discussion

Self-association of the anticancer antibiotic MTR is elucidated through a number of biophysical techniques. There have been preliminary reports of the association of the drug.[16] Self-association of several other antibiotics such as daunomycin,[17] CS-088,[18] amithiamycin D[19], amphotericin B,[20] and an analogue of actinomycin D[21] was reported earlier. However, these studies lack in-depth molecular characterization. However, this is the unique example of an anionic drug undergoing self-association overcoming the electrostatic repulsion among similar charges.

Here, we have employed diverse techniques to get a detailed picture of the process, including a quantitative estimation of

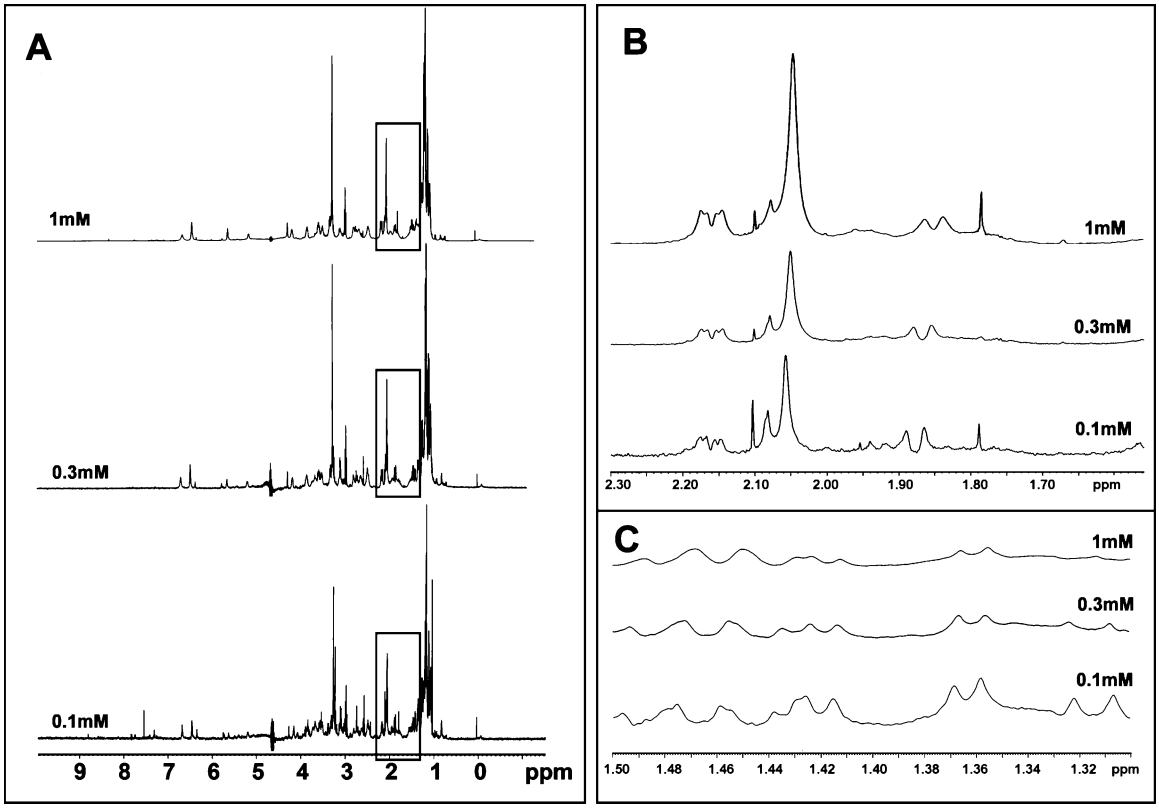

Figure 8. (A) 1D ^{1}H NMR spectra of $[(MTR)_2Mg^{2+}]$ at 1, 0.3, and 0.1 mM concentrations in 20 mM phosphate buffer, pH 8.0, at 25 °C. (B) Expanded region (1.5−2.3 ppm) to show the concentration dependence of the δ value of C7−CH_3. (C) Expanded region (1.3−1.5 ppm) to show the concentration dependence of the δ value of EC5″−CH_3.

the association. The experimental approaches adopted here are according to the concentration windows within which these techniques are applicable.

Different experimental approaches show the existence of different molecular species of the anionic drug molecule (MTR) in a concentration-dependent manner, even in the micromolar region. The significance of this observation lies in the fact that the drug interacts with its physiological targets within this range of concentrations. Moreover, the antibiotic is a natural product (produced by bacteria of the *Streptomyces* genus); the phenomenon of aggregation might further complicate its biosynthetic pathway as well as its storage phenomenon in the microorganism. Again, in the interpretation of the binding data of the anionic drug with its target, the total concentration of the drug is often equated to its molar concentration and hence over estimated, if the process of self-association is not taken into account.

Absorbance spectra in the concentration range of 5−200 μM provide the primary evidence of the self-association occurring between the drug molecules and also indicate the concentration ranges where the drug is supposed to exist as different molecular entities. A red shift in the spectrum occurs as a result of the interaction between the transition dipoles of the chromophores in the aggregated species. Absorbance also shows that the association is not well-defined in the case of the $[(MTR)_2Mg^{2+}]$ complex. Fluorescence quenching (Figure 3A) at a higher concentration of the anionic drug originates from the self-association of the anionic drug because the electronic environment of the fluorophore changes upon self-association, leading to a more efficient radiationless transition in the higher oligomer(s). The effect of the coupling between the transition dipoles of the chromophore in the oligomer with an increase in concentration becomes more apparent in the case of CD spectra (Figure 6A). Splitting of the bands is a result of the association-related coupling of the transition dipoles in the asymmetric environment.

Ideally, the molar heat of dilution of a specific molecule does not change in a concentration-dependent manner (as shown for EtBr and the neutral drug). In the case of anionic MTR at pH 8.0, we find a significant variation in the molar heat of dilution, thereby indicating the presence of secondary interactions. As there were no other molecular entities in the system, the phenomenon of self-association appears to be the plausible mechanism. Deviation of the emission intensity of anionic MTR at 540 nm from the expected linearity is also indicative of association. ITC and fluorimetric studies clearly illustrate that the anionic drug molecule self-associates around 20 μM.

DLS measurements confirm the association of MTR around the concentration mentioned above and supports the suggestion for dimerization because the effective hydrodynamic diameter of the species existing at 25 μM is about twice that of the species present at 6 μM. Lack of association of the drug−metal complex is also clear from the DLS measurements, which indicated the presence of a single type of molecular species.

The concentration dependence of the CD values justifies that higher-order associations occur at concentrations above 25 μM. Figure 6B shows two breaks; this leads us to propose a tetrameric model of association along the concentration range probed by CD (mentioned in section 3.5). The transition from trimer to tetramer takes places around 200 μM. Any further association beyond the tetramer is not obtained, as is also evident from chemical shift values in NMR. Inspection of Table 2 proves that dimerization is the predominant process, while loose association seems to be taking place between dimers at higher-concentration ranges.

The association could occur from the following sources: stacking interactions involving aromatic rings of the aglycone

part, hydrophobic interactions involving the sugar residues,[22] and hydrogen bonding via a bound water molecule and/or sugar residues. A priori, one might assume that the process of association is mediated by stacking interactions between the chromomycinone rings of several molecules. ITC data show that the neutral drug (pH 3.5) does not undergo association at higher concentrations. NMR results also indicate the absence of a significant upfield shift of the aromatic protons (C5−H and C10−H) with an increase in concentration. These two features suggest against stacking interactions involving an aromatic ring as a potential source of aggregation. Concentration-dependent resonances of the sugar protons as well as the methyl protons between the sugar moieties ($C7-CH_3$) are consistent with the proposition of the involvement of sugar residues during the process of self-association. This leads us to conclude that self-association is mediated through the sugar residues. Water might also play a role in the association. The process of association might be mediated through H bonding (via water molecules) among the potential loci in the sugar residues. Alternately, it might result from weak hydrophobic and/or hydrophilic self-interactions among the sugar residues as sugars are amphiphilic in nature, possessing both hydrophobic (carbon and hydrogen atoms) as well as hydrophilic faces (oxygen atoms).[22,23]

5. Conclusion

Our study has demonstrated the concentration-dependent formation of oligomers ($n = 2$ to 4) of anionic MTR ranging from the dimer to the tetramer over micromolar to millimolar concentration ranges. As mentioned in the Introduction, the self-association of MTR at and above physiological pH has possible implications in vivo. The aggregation involves participation of the sugar residues. From the chemical perspective, such involvement of sugar residues in the process of aggregation is an uncommon phenomenon reported for sugar-containing antibiotics. Another important feature stemming from the above studies is that the association of the anionic drug with Mg^{2+} leads to the $[(MTR)_2Mg^{2+}]$ complex, which does not undergo self-association.

Acknowledgment. The authors acknowledge Professor Manabendra Mukherjee, Surface Physics Division, SINP, for his permission to use the DLS instrument and Mojammel Haque Mondal for his technical assistance. We acknowledge Dr. Siddharta Roy, Director, Indian Institute of Chemical Biology (IICB), and E. Padmanabhan of the NMR facility, Indian Institute of Chemical Biology (IICB), Kolkata. S.L., P.G.D., and P.M. contributed equally to the work.

Supporting Information Available: 1D and 2D (NOESY) spectra of anionic MTR (1 mM) and the $[(MTR)_2Mg^{2+}]$ complex (1 mM MTR containing 10 mM Mg^{2+}]. This information is available free of charge via the Internet at http://pubs.acs.org.

References and Notes

(1) Calabresi, P., Chabner, B. A., Hardman, J. G., Limbard, L. E., Eds. *Goodman and Gilman's The Pharmacological Basis of Therapeutics: Chemotherapy of Neoplastic Diseases*, 9th ed.; Macmillan: New York, 1991; pp 1225−1269.

(2) Wohlert, S. E.; Kunzel, E.; Machinek, R.; Mendez, C.; Salas, J. A.; Rohr, J. *J. Nat. Prod.* **1999**, *62*, 119−121.

(3) Dimaraco, A., Arcamone, F., Zunino, F., Corcoran, J. W., Hahn, F. E., Eds.; *Antibiotics, Mechanism of Action of Antimicrobial & Antitumor Agents*; Springer: Berlin, Heidelberg, New York, 1975; pp 101−128.

(4) Goldberg, I. H.; Friedmann, P. A. *Annu. Rev. Biochem.* **1971**, *40*, 775−810.

(5) Hou, M. H.; Wang, A. H. *Nucleic Acids Res.* **2005**, *33*, 1352−1361.

(6) Snyder, R. C.; Ray, R.; Blume, S.; Miller, D. M. *Biochemistry* **1991**, *30*, 4290−4297.

(7) Fibach, E.; Bianchi, N.; Borgatti, M.; Prus, E.; Gambari, R. *Blood* **2003**, *102*, 1276−1281.

(8) Liacini, A.; Sylvester, J.; Li, W. Q.; Zafarullah, M. *Arthritis Res. Ther.* **2005**, *7*, 777−783.

(9) Ferrante, R. J.; Ryu, H.; Kubilus, J. K.; D'Mello, S.; Sugars, K. L.; Lee, J.; Lu, P.; Smith, K.; Browne, S.; Beal, M. F.; Kristal, B. S.; Stavrovskaya, I. G.; Hewett, S.; Rubinsztein, C. D.; Langley, B.; Ratan, R. R. *J. Neurosci.* **2004**, *24*, 10335−10342.

(10) Lin, R. K.; Hsu, C. H.; Wang, Y. C. *Anti-Cancer Drugs* **2007**, *18*, 1158−1164.

(11) Aich, P.; Dasgupta, D. *Biochemistry* **1995**, *34*, 1376−85.

(12) Sharma, A.; Schulman, S. G. *Introduction to Fluorescence Spectroscopy*; Wiley Interscience: New York, 1999; pp 20−23.

(13) Martin, S. R. *Biopolymers* **1980**, *19*, 713−721.

(14) Devi, P. G.; Pal, S.; Banerjee, R.; Dasgupta, D. *J. Inorg. Biochem.* **2007**, *101*, 127−137.

(15) Krishna, N. R.; Miller, D. M.; Sakai, T. T. *J. Antibiot. (Tokyo)* **1990**, *43*, 1543−1552.

(16) Keniry, M. A.; Owen, E. A.; Shafer, R. H. *Biopolymers* **2000**, *54*, 104−14.

(17) Chaires, J. B.; Dattagupta, N.; Crothers, D. M. *Biochemistry* **1982**, *21*, 3927−3932.

(18) Kikuchi, T.; Ito, N.; Suzuki, M.; Kusai, A.; Iseki, K.; Sasaki, H. *Int. J. Pharm.* **2005**, *299*, 100−106.

(19) Lewis, R. J.; Hughes, R. A.; Alcaraz, L.; Thompson, S. P.; Moody, C. J. *Chem. Commun.* **2006**, *40*, 4215−4217.

(20) Grijalba, M. T.; Cheron, M.; Borowski, E.; Bolard, J.; Schreier, S. *Biochim. Biophys. Acta* **2006**, *1760*, 973−979.

(21) Veselkov, D. A.; Lantushenko, A. O.; Davies, D. B.; Veselkov, A. N. *Russ. J. Bioorg. Chem.* **2002**, *28*, 342−347.

(22) Patel, T. R.; Harding, S. E.; Ebringerova, A.; Deszczynski, M.; Hromadhova, Z.; Togola, A.; Paulsen, B. S.; Morris, G. A.; Rowe, A. J. *Biophys. J.* **2007**, *93*, 741−749.

(23) Santacroce, P. V.; Basu, A. *Glycoconjugate J.* **2004**, *21*, 89−95.